Annual Report

Improved Passive Microwave Sounding of the Atmosphere

NASA Grant NAG 5-2545

covering the period

March 15, 1995 - March 14, 1996

submitted by

D. H. Staelin

P. W. Rosenkranz

M. J. Schwartz

July 2, 1996

Abstract

The effort this year focused primarily on 118-GHz transmittance experiments. The data analyzed here was collected with the Microwave Temperature Sounder (MTS) radiometer package during the CAMEX deployment of 1993 with the aim of validating current models of atmospheric microwave absorption in the O_2 bands near 54 and 118 GHz. Particular attention has been paid to data collected during four flights when the MTS scanned zenith while profiles of downwelling radiances were collected through ascents and descents. These radiances, in conjunction with radiosonde temperature data, permit the retrieval of band-averaged absorption profiles for each channel.

The Millimeter-wave Propagation Model (MPM92) provides theoretical expressions for the absorption of microwaves by oxygen and water vapor and accounts for the interference of pressure-broadened spectral lines[1]. This model is a good fit to laboratory measurements at temperatures ranging from 279-327 K, but it has been suggested that extrapolation to the conditions of the atmospheric tropopause may result in underestimation of absorption by as much as 15%[2].

Preliminary results of the analysis of MTS data appear to be in general agreement with the predictions of the MPM model to within the accuracy of the measurements, which through the coldest parts of the atmosphere ranges from less than ±5% in the most opaque channels to greater than ±10% in the most transparent channels. At those altitudes where each channel is most sensitive to changes in absorption, there is some indication that the modeled absorption may be biased low relative to the observations. Accurate instrument calibration provided challenges, particularly when observed radiances were as much as 260 K below the temperatures of the cold calibration load.

---

[1] H.J.Liebe, P.W.Rosenkranz, G.A.Hufford, Atmospheric 60-GHz Oxygen Spectrum: New Laboratory Measurements and Line Parameters. J.Quant Spectrosc. Radiat. Transfer, Vol 48, No. 5/6, 1992

[2] A.J.Gasiewski, Ph.D. Thesis, Dept. of Electrical Engineering and Computer Science, MIT, Dec., 1988

1. Overview of MTS 118-GHz Transmittance Measurements

MTS zenith-viewed measurements are particularly sensitive to changes in atmospheric attenuation at those levels where space-based nadir-viewing weighting functions peak (see Figure 1), since in the top scale height of the atmosphere zenith brightness temperatures drop sharply, from values comparable to the atmosphere's physical temperature to values approaching the cosmic background temperature, 2.7 K.

The zenith-viewing configuration avoids the need to model variable earth-surface emissivity, roughness, and temperature and eliminates contributions of the highly variable lower troposphere from all but the lowest altitude observations. Variable surface emissivity results in upwelling radiances composed of varying fractions of the two sets of curves on the left of Figure 2; the dashed lines are upwelling radiance above a perfectly black surface (emissivity of 1) and the solid lines are upwelling radiance above a perfectly reflecting surface (emissivity of 0). Observed down-welling radiance fields in the upper troposphere and above should be well modeled as smooth functions of frequency, pressure, and angle from zenith, calculated from a horizontally-stratified, planar-symmetric atmospheric model.

The following discussion includes recently-made improvements to the instrument model, calibration corrections, consideration of the accuracy of ancillary data sets, fitting and smoothing of radiance data, and the inference of absorption coefficients from profile data. Retrieved absorption profiles are compared to the predictions of the Millimeter-wave Propagation Model (MPM92) developed by Liebe and Rosenkranz in regimes where its accuracy has been questioned.

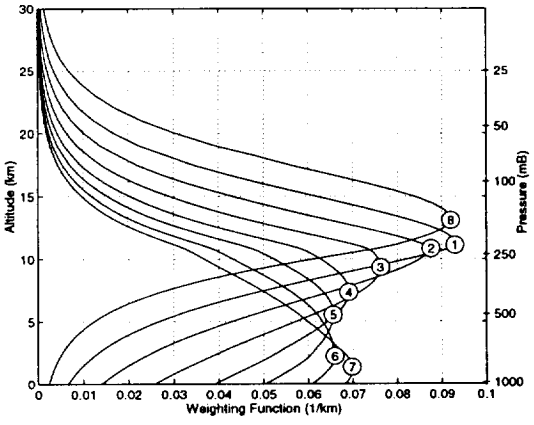

Figure 1. Weighting functions for nadirial views from space through a standard 1976 US atmosphere with black surface, calculated with the MPM92 absorption model for the eight MTS channels near 118.75 GHz.

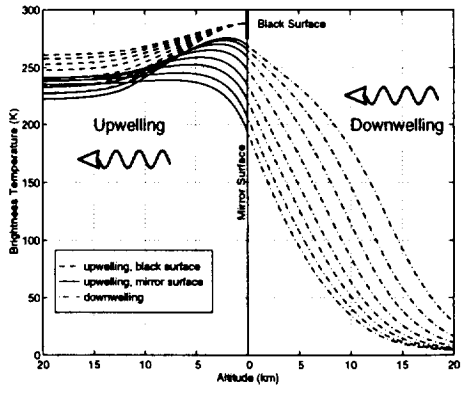

Figure 2. Upwelling and downwelling brightness temperatures for MTS 118-GHz channels, U.S.Std1976 Atmosphere and MPM92 absorption model.

2. Modeling of Data

Work has been done previously to model the MTS data by assuming the MPM92 model of atmospheric absorption is accurate, using the most nearly coincident radiosonde data available to do radiative transfer calculations and by producing simulated MTS observations which accurately integrate radiances across channel passbands, and are interpolated to the viewing pressure level and orientation of each observation. Such simulated data can then be compared to the actual observations to check for consistency.

In the work described here, this approach is avoided. No assumptions are made about the adequacy of any particular absorption model, beyond the transparency approximation assumed in cold-space calibration, above. The assumption made is that the data for each channel, for each ascent or descent, can be reasonably approximated by a smooth function of pressure level and viewing angle from zenith. If this surface can be determined from the data, absorption can be inferred from its differential structure, though it should be noted that the nonlinearity of the equation of radiative transfer with respect to absorption coefficient may cause these channel band absorptions to differ from the linear band-weighted average absorptions.

Accurate modeling requires accurate ancillary data: aircraft pressure level, pitch, and roll, as well as precise knowledge of the scan mirror's pointing relative to the aircraft. A great deal of effort was invested in attempts to confirm these data's accuracy, in the synchronization of drifting clocks (both in the MTS and in the ER-2's navigation system), and in the interpolation of the data stream from the aircraft's navigation system to the times of observations with sub-second accuracy. Despite this care there are significant uncertainties in these data. The accuracy of the navigation data from the ER-2's air-data computer provided during CAMEX and previous deployments, particularly that of the altitude measurement, is an open question. Estimates by aircraft personnel of altitude errors are typically in the range of 100 m, although there seems to be no systematic calibration of the altimeter and the swapping out of components of the system mid-deployment may somewhat confound any such attempts.

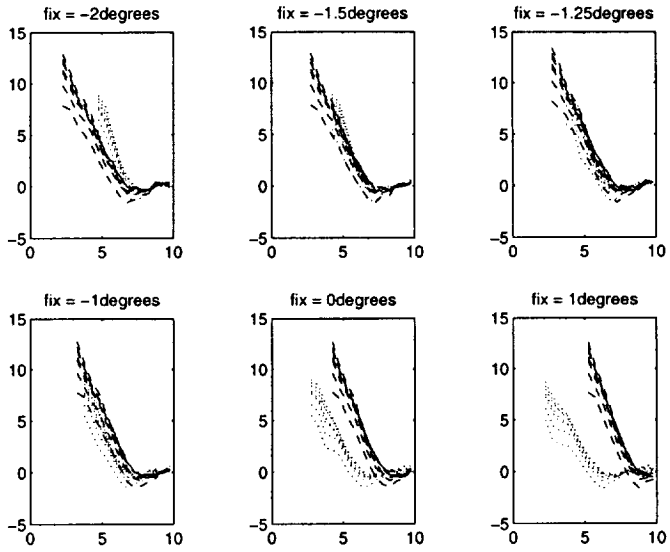

Figure 3. The disk of the sun passing through the beam on the 10-07-93 ferry flight provides an opportunity to confirm/correct beam-pointing data.. The dashed lines are spot-1 data, and the dotted lines are spot-2 data. A correction of ~1.25° to the roll makes the sun's warming have the same angular dependence for the two scan positions.

The altitude measurement, such as it is, is actually a pressure measurement reported in units of kilometers referenced to the 1976 Standard U.S. atmosphere. Certainly, naive belief that the reported values are altitudes can lead to errors of many hundreds of meters in a tropical atmosphere. Comparison of the ER-2's pressure-altitude measurement with actual altitude measurements inferred from surface returns to the EDOP RADAR (operated briefly during a CAMEX flight,) is consistent with the 100-m estimate. Unfortunately, RADAR data was not available in conjunction with a radiosonde temperature profile, so the exact relationship of altitude and pressure was not known.

An opportunity to confirm the accuracy of the pointing data was afforded by an extended section of the ferry flight (10-07-93), during which the sun was in the plane of the scan mirror and repeatedly passed through the MTS beam. A bit of matrix algebra transforms the known position of the sun into aircraft coordinates. The effect of the sun on antenna temperatures of two scan positions could be readily discerned from the relatively stable brightness baseline of level, high-altitude flight, confirming the sun's position between these two spots. Assuming a symmetric antenna pattern, a correction was determined to the combined aircraft roll and mirror scan position such that the warming as a function of angle from the sun was consistent in the two mirror positions, as is seen in Figure 3. This presumed small (1.25°) error in pointing could be due to error in reported aircraft roll, in mounting of the MTS scanhead in the wing pod, in flexure of the wing, or in homing of

the scan mirror. Lacking any other candidates, this correction was made to the roll measurement of all CAMEX data sets. Such a correction will result in negligible changes in modeled brightness temperatures near zenith, but could be significant at high scan angles due to the nonlinearity of secant. No method of confirming the pitch angle has been determined.

3. Fitting of Surface to Radiance Data

3.1 Least square fit to a smooth surface

The observed brightness temperature for each channel is expected to be a smooth, 2-dimensional function of aircraft altitude (pressure level) and of angle of the observation from zenith. Pressure (H) is conveniently labeled in units of km for the standard US 1976 atmosphere (these are the units of "pressure altitude" returned by the ER-2 navigation system.) The secant of the zenith angle (s) is a natural unit for the other degree of freedom since the pathlength of a ray through a planar, horizontal slab of atmosphere is proportional to this quantity. The desired calibrated output of an MTS ascent or descent is a 2-dimensional surface, $T_B(ch; H,s)$, with error bars. Such a surface fit is particularly useful when one is interested in the differential structure of the profile.

MTS data collected during ascents and descents is not uniformly sampled in either altitude or in viewing-angle from zenith, so fitting a surface to the data is somewhat problematic. The data is both noisy and "clumpy, " so that binning by H and s is not the ideal way to smooth the data. Care is taken to synchronize clocks and to interpolate aircraft 1-s navigation data (including pressure-altitude, pitch and roll) to the precise times of observations, and this information should be taken into account in the fitting process.

The model adopted for this data reduction is the linear interpolation of a rectangular grid, typically 21 levels of H (0-20 km) by four values of s (1 to 1.6). The values of brightness at these 84 grid points are the parameters of the model, and the best-fit surface is that which minimizes a weighted sum of the difference between the MTS data and the interpolated grid, subject to an additional cost for grid curvature. Apart from proper weighting, it is straightforward to set up the matrix equation to be solved.

The grid values are unwrapped for successive values of s into a column vector $\mathbf{g}$, and the bilateral interpolation of the grid to N observation points $\mathbf{z}$ is expressed as multiplication by a Nx84 matrix $\mathbf{A}$ with 4N nonzero elements $\mathbf{z} = \mathbf{Ag}$. If the error covariance Λ_{zz} of the observations $\mathbf{z}$ is known, the cost to be minimized for a least-square error fit E_{fit} may be expressed as

$$E_{fit} = (\mathbf{Ag} - \mathbf{z})^T \Lambda_{zz}^{-1} (\mathbf{Ag} - \mathbf{z})$$

$$\frac{\partial E_{fit}}{\partial \mathbf{g}} = 2\mathbf{A}^T \Lambda_{zz}^{-1} (\mathbf{Ag} - \mathbf{z})$$

The costs for curvature in the H and s directions, taken to be the sums of the rate of change of slope at each interior grid point, may each be written as a multiplication by tri-diagonal 84x84 matrices. The partial derivatives of these costs with respect to the elements of **g** are given by matrix multiplications $\mathbf{C_H}\,\mathbf{g}$ and $\mathbf{C_s}\,\mathbf{g}$, where each matrix **C** has 5 nonzero diagonals. Scalar multiplicative tension factors T_H and Ts may be adjusted to stiffen the surface independently in the two directions.

$$\frac{\partial E_{curvature}}{\partial \mathbf{g}} = (T_H \mathbf{C_H} + T_s \mathbf{C_s})\mathbf{g}$$

Setting the partial derivative of the total cost $E = E_{fit} + E_{curvature}$ with respect to the elements of **g** to zero and solving for **g** gives

$$\mathbf{g} = \left(\mathbf{A}^T \Lambda_{zz}^{-1} \mathbf{A} + \mathbf{C_H} + \mathbf{C_s}\right) \backslash \mathbf{A}^T \Lambda_{zz}^{-1} \mathbf{z}. \qquad \text{(Eqn. 1)}$$

The difficulty in this fitting process comes in dealing with correlated errors. For uncorrelated errors (diagonal Λ_{zz}), points are weighted by their inverse variance. However, errors in calibrated antenna temperatures, as estimated in Section 6.1, are known to be correlated since individual calibration observations are used repeatedly. Filtering of calibration counts, necessary to bring calibration errors down to reasonable values, (particularly when calibrated temperatures are far from those of the calibration loads), increases the spread of this correlation. Exact solution of the expression for **g** involves matrix division by what is typically a 4000×4000 correlation matrix with 240 non-zero diagonals, and is computationally impractical. In the treatment described here, correlation of the errors was ignored in fitting the surface, but was considered in the estimation of the error bars on the grid values.

3.2 Estimation of attenuation

For a thermally emitting, nonscattering atmosphere, the differential transfer equation governing intensity (power per unit area at a specific frequency (ν), in a particular direction (dΩ), and altitude (h)) allows the absorption coefficient to be directly determined from a physical temperature profile and the intensity profile. With intensity conveniently expressed in units of Kelvins ($2k_B \nu^2/c^2 = 1$), and assuming the Rayleigh-Jeans limit, the transfer equation governing changes in brightness temperature T_B with altitude h is

$$\frac{dT_B}{dh} = \alpha_v \sec\phi\left(T_{\text{phys}} - T_B\right)$$

$$\alpha_v = \frac{\frac{dT_B}{dh}}{\sec\phi\left(T_{\text{phys}} - T_B\right)} \qquad \text{(Eqn. 2)}$$

where α_v is the absorption coefficient, with units of Np/km. T_{phys} and α_v are assumed to be functions of altitude (h) only. T_B is a function of altitude and viewing angle (h, ϕ), and diffraction is considered negligible so that ϕ may be considered constant along a ray.

Attempts to retrieve attenuation profiles from MTS data are complicated by the fact that its channels have broad bandwidths, typically on the order of 200 MHz. If absorption varies significantly across a channel passband, the retrieved absorption estimated above will not be the linear passband-weighted average of discrete-frequency absorption, since the transfer equation is nonlinear. An attempt was made to include the effects of this nonlinearity in the band-averaging of model absorption when comparing retrieved absorption with theoretical expressions based upon radiosonde profiles. The model is used to produce simulated radiance data in 10-MHz steps across the MTS band which are averaged with appropriate channel passband filters to produce simulated MTS channel data. Absorption is retrieved from this simulated channel data in the same way that it is retrieved from the actual data; nonlinear effects should be similar in both cases and are expected to approximately cancel when differences between observed and simulated absorption are considered.

4. Interpretation of Results

4.1 Comparison of Retrieved Absorption with MPM Model

Absorption coefficients inferred above are compared to the predictions of the MPM 92 model. Starting with a radiosonde profile (altitude, temperature, pressure, and water vapor densities of the column through which the observations were made), the MPM model is used to calculate absorption. A forward radiative transfer calculation is done on a grid of altitudes (no steps larger than 10 mB or 1 km) and zenith angles (typically 5 linear steps in secant) for 10-MHz steps across the MTS ~4-GHz passband. This table is integrated against the MTS double-sideband channel passbands and interpolated to the actual observation pressure levels and secants of the flight-data observations. Absorption is estimated from the resulting simulated MTS data in the same way that it is estimated from the actual flight data, minimizing the impact of any biases resulting from the surface fitting and absorption coefficient estimation processes.

Figure 4 and Figure 5 are composites of data collected during 3 ascents and 3 descents on the four upward-looking CAMEX flights. One ascent was excluded from the analysis due to instrument instability and lack of a proximal radiosonde. One descent was excluded because of heavy cloud cover. Theoretical and observed absorption profiles from the six included transits were averaged at each altitude level, weighted by their inferred variances. Error bars shown include both the uncertainties in individual estimates and the effects of the differences in atmospheric profiles.

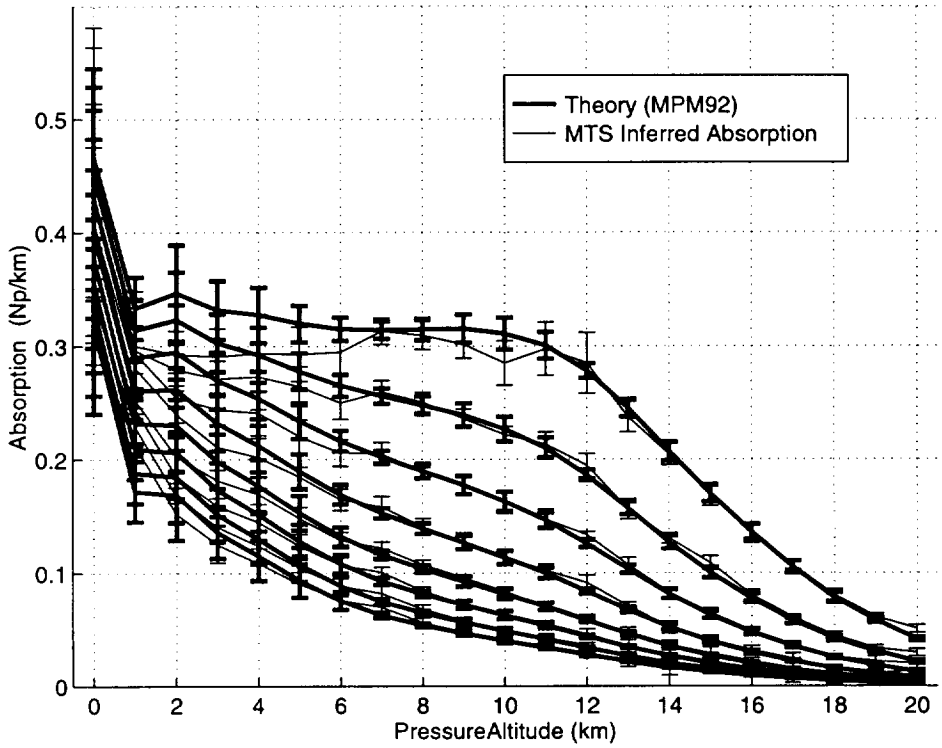

Figure 4. Retrieved absorption for the 8 MTS channels, and corresponding predictions of the MPM92 absorption model averaged over six CAMEX atmospheric transits.

Retrieved absorptions are expected to be most reliable at levels near where the temperature weighting functions peak, where transmittance to space is dropping sharply for a given channel. At these levels, brightness temperatures are changing rapidly but are still well removed from the physical temperature of the level. At still higher levels, the rate of change of brightness temperature with altitude is small compared to its uncertainty, and at lower altitudes, (T_{phys} - T_B) may be small compared to its uncertainty. Large fractional errors at the highest altitudes in the most opaque channels (8,1-3) are apparently an artifact of the fitting process, although this is still under investigation. Errors below 6 km reflect both uncertainties in water vapor and temperature profiles and the inability of the surface fit to resolve sharp changes in brightness temperature associated with temperature inversions in some of the profiles.

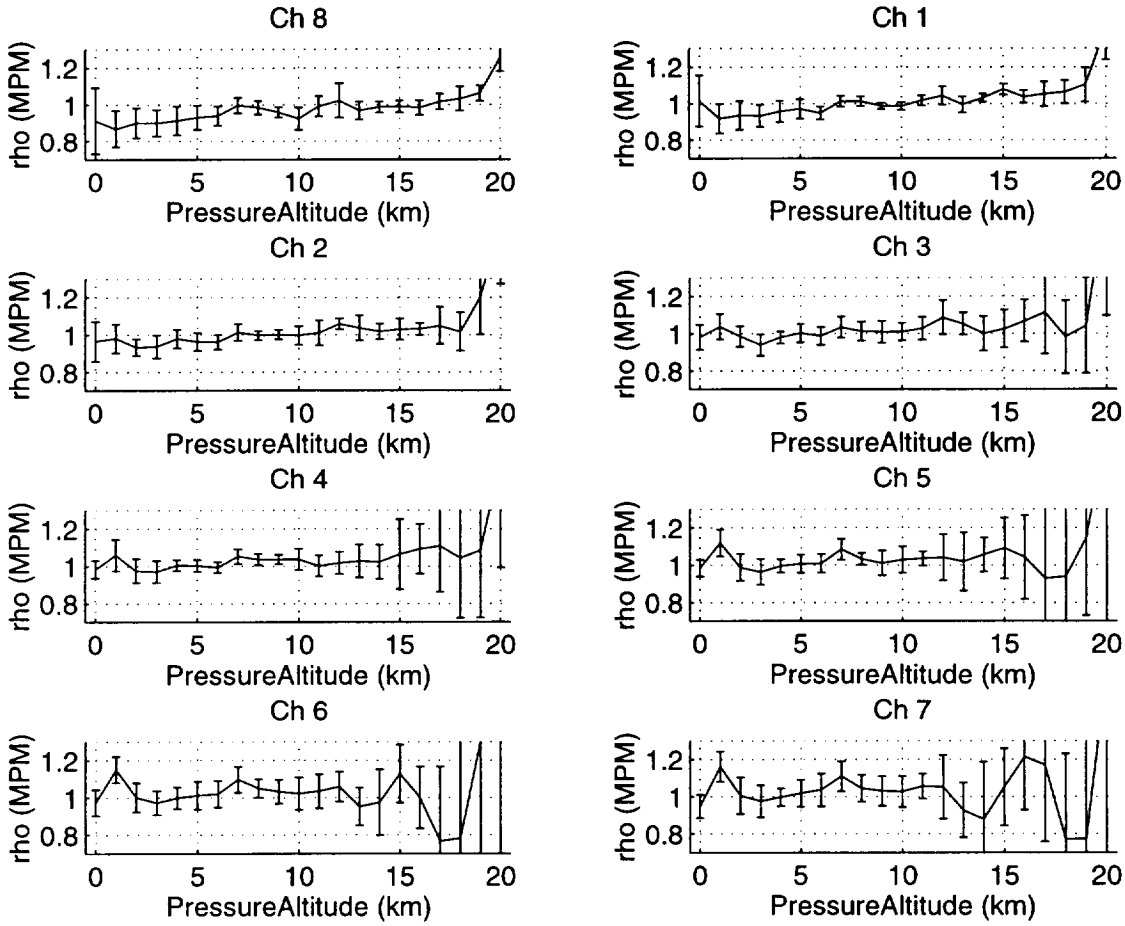

Figure 5. The ratio of retrieved to modeled absorption for the eight MTS 118-GHz channels, averaged over six zenith-viewing ascents and descents. Large fractional errors in transparent channels at high altitudes are to be expected, since estimated rates of change of brightness with altitude are small compared to brightness uncertainty.

In summary, these observations appear to be consistent with the MPM model for the levels at which they are considered most reliable. which are from approximately 8 to 18 km for the most opaque channel (8) and approximately 3 to 12 km for the most transparent (7). Figure 5 shows that the ratio of retrieved to modeled absorption averaged for each pressure-level over the CAMEX flights. Pressure altitude refers to pressure levels labeled with their corresponding altitudes in the U.S. Standard 1976 atmosphere.

Inferred absorption at lower altitudes in the most opaque channels is consistantly lower than is predicted by theory. This disagreement may be an artifact of the coarse method used to extract antenna temperature derivatives with altitude or the result of systematic errors in the aircraft altitude. Further analysis is required before any geophysical significance is assigned to these measurements.

5. MTS 118-GHz Instrument

5.1 Instrument Description

The Millimeter-wave Temperature Sounder (MTS) includes two radiometers, one with eight channels near 118 GHz and the second with a single, tunable double-sideband passband near 54 GHz. The package also includes a wide-angle CCD video camera. This discussion concerns the 118-GHz instrument, a cross-track scanning microwave spectrometer with eight double-sideband channels within 2 GHz of the oxygen resonance at 118.75 GHz. This Dicke radiometer has a stationary scalar feed horn and fixed subreflector with a 7.5^{o} beamwidth viewing a scanned mirror. All views are chopped at 25 Hz against an ambient temperature Dicke reference load. Symmetric sidebands 330 to 2030 MHz from the resonance are mixed into a common intermediate-frequency section (IF) from which eight channels are filtered and synchronously detected. Fourteen spots within $\pm 46.8^{o}$ of nadir, a heated target, and an ambient temperature calibration target are viewed during each 5.5-second scan.. The package is typically flown on a NASA ER-2 high-altitude aircraft and may be mounted in either nadir-scanning or zenith-scanning orientations. This is substantially the same instrument as described by Gasiewski *et al.* [3] with the following changes:

- The IF amplifiers were replaced
- The filter bank was repackaged
- The computer control was replaced
- The post-detection video amplifiers were removed
- Filter values on synchronous detector inputs were adjusted

---

[3] A. J. Gasiewski, J.W. Barrett, P.G.Bonanni and D. H. Staelin, Aircraft-based Radiometric Imaging of Tropospheric Temperature and Precipitation Using the 118.75-GHz Oxygen Resonance, Journal of Applied Meteorology, Vol. 29, No. 7, July 1990

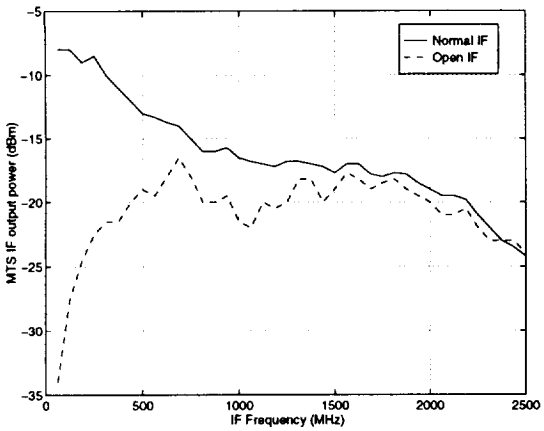

Figure 6. 118-GHz IF power output with intermittent contact open and closed. The open state has enough capacitance to pass higher frequencies, while blocking DC.

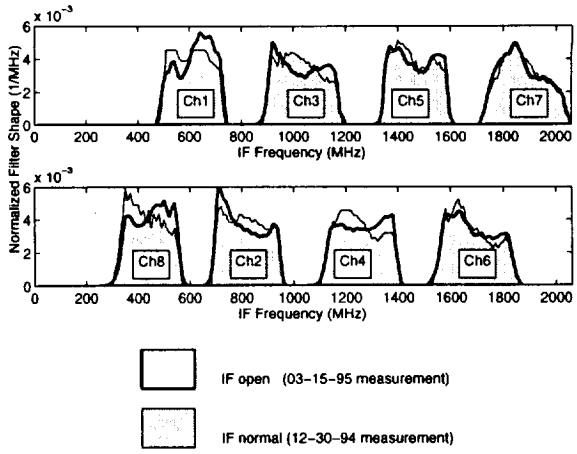

Figure 7. Normalized MTS 118-GHz passbands for the two gain states. Changes in individual channel passband shapes must be accounted for in instrument modeling.

5.2 IF Intermittent Contact

An intermittent contact in an SMA connector of a cable on the output of the last amplifier in the IF section of the 118-GHz radiometer has apparently plagued this system for several deployments, giving rise to two distinct states with significantly different channel gains and passband shapes. Sharp discontinuities in system gain have been noted during some flights since the CAPE missions of 1990, but there was difficulty replicating these transitions in the lab. During the CAMEX deployment, the in-flight state of the contact became more consistently "open," and the defective connector was subsequently identified and spectrum analyzer measurements of both states were made in the lab. When in its "open" state, there is enough capacitance within the defective connector that it functions as a high-pass filter with all radiometer channels above its cutoff frequency, as is apparent in Figure 6.

In laboratory measurements, the impedance mismatch of the open contact at the output of the last IF amplifier resulted in a standing wave on the line between the front end and the filter bank. Spectrum analyzer measurements showed a ~30 MHz ripple with peak-to-peak amplitude varying from 10 to 18 dB. Standing waves may also have been present in the flight package as installed in the aircraft, but differences in cabling and bulkhead connections between the two configurations make interpretation of this fine structure a questionable enterprise. In that the channel passbands are on the order of 200 MHz wide, fine structure in the response as a function of frequency is not expected to change band-averaged radiances significantly. The dashed line of Figure 6 is actually a low-pass filtered (in frequency) version of the linear response of the bandpass filtered output of each channel for a thermal, 290 K antenna temperature.

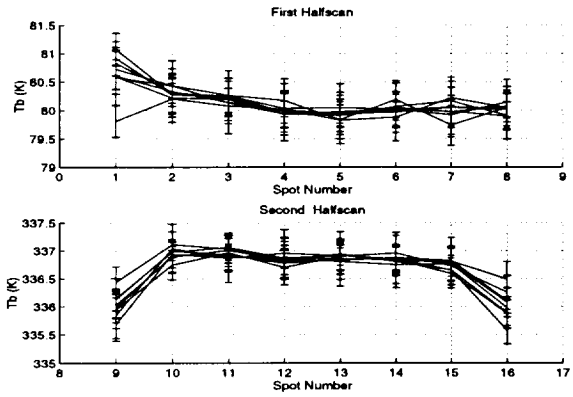

Figure 8. 118-GHz memory in laboratory liquid nitrogen observations. Transitions are not sharp after ~260 K input discontinuity. The slight trend in the second through fifth spot of each group is not understood. Anomalous spot-16 data is due to interference from the 53-GHz radiometer.

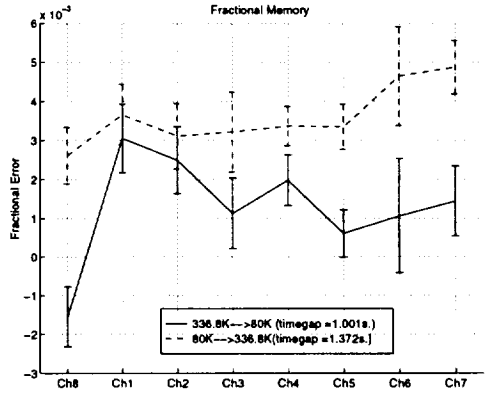

Figure 9. Fractional memory for MTS 118-GHz channels as determined from laboratory measurements. A single value, 0.003, was used for all channels in the CAMEX data reduction.

Since calibration measurements are made throughout a data flight, calibration of the instrument may be achieved on both sides of isolated sharp changes in a channel's gain. Care must be taken not to filter calibration measurements in a way that averages across such discontinuities. A subtler, but finally more persistent effect of the intermittent contact is that the shape of normalized channel passbands is dependent upon contact state, as is apparent from Figure 7. The resultant shifts in passbands are expected to produce changes in brightness temperature as large as several K, and must be taken into account in careful modeling of the instrument.

5.3 Time-Series Interference

Laboratory measurements consisting of alternated blocks of repeated observations of the hot calibration load and of a piece of absorber immersed in liquid nitrogen reveal a small amount of memory in the 118-GHz system. The resulting square wave of ~260 K is perceptibly rounded, with the first observation after a jump retaining approximately 0.3% of the preceding observation. In Figure 9, the value to which a group of 8 observations eventually settles was set to the known thermocouple temperature for the hot load and to 80 K for the liquid nitrogen.

At least some part of this memory effect is due to high-pass filters on the input to the synchronous detection cards which are the back end of the Dicke detection system. However, the modeling and correction of this time-series interference has proven to be difficult. The interference does not seem to be a simple decay with a single time constant. There is a slight downward trend in repeated measurements both after a jump upward and

after a jump downward. This asymmetry somewhat confounds determination of the baseline and may account for the disagreement of the two lines in Figure 9. The exact time sequence of scenes viewed as the mirror moves between scan positions is unknown. Dicke switching results in output counts which are actually differences between interleaved observations of the antenna and of a reference load, and modeling of the response of this coarse differentiator to a switched, decaying input is somewhat involved.

Fortunately, the fractional magnitude of the interference is small enough that it has a perceptible effect only after large jumps in observed brightness. In flight configuration, the scan pattern consists of 14 sky observations, a view of the cold load (T_C=260-300 K), and a view of the hot load (T_H = 335 K). The hot load counts would be biased cold on the order of 0.3% of the calibration load temperature difference, or as much as 0.2 K. Larger errors would be expected in the cold load counts and in the first spot after the hot load observation, in cases where the sky temperature is extremely cold. The jump from sky to cold load may be on the order of 260 K, and hot load to sky of 330 K with estimated resulting memory biases of 0.8 K and 1 K respectively.

A first order correction was made to all of the raw, 118-GHz data sets to make a rough correction for the time-series interference. A fixed fraction (0.003) of the difference between each measurement and its predecessor was added to each measurement. Further adjustment of the linear calibration, based upon observations of the cosmic background through an approximately transparent atmosphere during the highest altitude portions of flights (discussed below) will correct for most of the inadequacy of this crude correction. The first observation after calibration is susceptible to the largest errors, and because more reliable, redundant measurements at the same angle from zenith are typically made at the other end of the scan, this first spot is excluded from the following analysis.

The suppression of spot 16's observation by ~0.7 K was traced to interference from the signals used to control the ferrite switches in the 54-GHz radiometer. The ferrite switches allow this radiometer to view its antenna and internal hot and cold loads and to Dicke switch synchronously with the 118-GHz system. The interference is likely a ground-loop problem, and may not have been present during flight, since chassis grounding in the lab was necessarily quite different from that of the flight configuration.

If this interference is present in flight, it would systematically bias all observations of the 118-GHz hot load, since all 118-GHz calibration measurements were concurrent with those of the 54-GHz instrument. Such systematic suppression of 118-GHz hot-load counts is a potential source of serious errors when extrapolating the calibration line far from the reference load temperatures. Correction for such errors is discussed below, in section 6.2.

An attempt was made to quantify the memory problems in flight data through analysis of the scan asymmetry. The anomalous warming of the first cold-sky spot observed after calibration was evident in some of the data, but difficult to quantify since it is masked by geophysical limb-brightening effects which are sensitive to small uncertainties in scan/roll position.

6. Calibration

6.1 Ideal Linear Calibration

Calibration of MTS data is achieved though the observation of a heated and an ambient temperature calibration load at the end of each 5.5-s scan. With a presumption of linear radiometer response to received power, a calibration relation can be determined from cold (C) and hot (H) calibration load radiometric A/D "counts", and corresponding thermocouple measurements of the loads' physical temperatures (T_C , T_H). For an observation, A, this simple assumption gives an estimated, calibrated antenna temperature,

$$\hat{T}_A = \left(\frac{\hat{T}_H - \hat{T}_C}{H - C} \right) \cdot (A - C) + \hat{T}_C \qquad \text{(Eqn. 3)}$$
$$= gA + b$$

where $g \equiv \dfrac{\hat{T}_H - \hat{T}_C}{H - C}$ and $b \equiv \dfrac{\hat{T}_C H - \hat{T}_H C}{H - C}$.

First order errors in calibration from errors in counts (δ_H , δ_C , δ_A,) and in thermocouple measurements (δ_{T_C} , δ_{T_H}) are

$$\Delta\hat{T}_A^2 = M_H{}^2 \left(g\delta_H + \delta_{T_H} \right)^2 + M_C{}^2 \left(g\delta_C + \delta_{T_C} \right)^2 + \left(g\delta_A \right)^2 \qquad \text{(Eqn. 4)}$$

where $M_H \equiv \dfrac{A - C}{H - C}$ and $M_C \equiv \dfrac{A - H}{H - C}$.

The temperatures of the calibration loads vary slowly compared to the rate at which thermocouple measurements are made, and the high-frequency RMS noise variation of these measurements is typically less than 0.1K. Low-pass filtering makes the effect of this noise negligible, however presumably redundant thermocouples typically have systematic disagreements on the order of 0.3 K. Systematic errors in thermocouple measurements, whether due to inaccuracies in the measurement or due to thermal gradients in the corrugated absorber material, will result in errors which will be considered below. For a nominal MTS channel bandwidth B, integration time τ, and receiver temperature T_R ,

$$g\delta_A \cong \Delta T_{\text{rms}} = \frac{2(T_R + T_A)}{\sqrt{B\tau}} \cong \vartheta\left\{\frac{2\cdot(1500K + 200K)}{\sqrt{2\cdot 200MHz\cdot 0.2s}}\right\} = 0.3K \qquad \text{(Eqn. 5)}$$

Since calibration load temperatures and the system's response parameters are generally slowly varying, the system temperature may be estimated from the high-frequency variation in observations of calibration load counts, scaled by a window-averaged g. A time-windowed estimate of the system noise, ΔT_{RMS}, is determined in this way for each channel and, under the assumption that the receiver temperature T_R is only slowly varying in time, the total calibration error is estimated using Eqn 4.

Given the slow rate of change of calibration counts C and H, errors δ_C and δ_H may be reduced by lowpass filtering in time. A boxcar of length N=20 used on this data increases integration time (τ) to 4s, reducing δ_H and δ_C by $\sqrt{N}$. However, when calibrating zenith, "cold-space" observations from high altitudes, M_C and M_H may be as large as 6 or 7. In such cases, the noise in calibrated antenna temperatures is still dominated by uncertainty in the observation of the calibration loads, and correlation of these errors, which is increased by filtering, complicates further data reduction. The lower two curves of Figure 10 show that for an ideal, linear MTS, filtering of the calibration counts by a boxcar of length 20 reduces calibration error to less than 1 K, but it should be noted that such errors will be correlated over 20 scans, which is approximately 2 minutes of data. Estimates of calibration noise covariance are used in the fitting of a surface to the data, as discussed below.

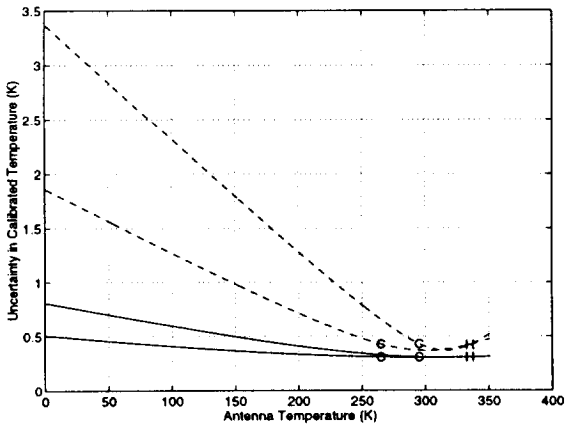

Figure 10. Calibration error for an ideal, linear radiometer with $\Delta T_{RMS} = 0.3$ K. Dashed lines are for unfiltered calibration measurements; solid lines are for a boxcar of length 20. $T_H = 335$ K in all cases. Pairs of curves show how errors are reduced when T_C is lowered from 295 K to 265 K, spanning the nominal range of cold load temperatures in flight.

6.2 Corrections to Linear Calibration

Simple, linear calibration of zenith-scanned MTS data using the instrument's heated and ambient-temperature calibration loads is inadequate when the antenna temperatures to be calibrated approach the 2.7-K cosmic background temperature. Not only are random calibration fluctuations magnified by extrapolation, but systematic errors result in nonphysical mean values below absolute zero. Fortunately, these coldest, highest altitude zenith antenna temperatures can be determined from theoretical considerations in ways that are relatively insensitive to errors in the attenuation model. Knowledge of systematic problems in calibration for these coldest observations can then be used to develop a reasonable correction for the data set as a whole.

6.2.1 Cold-Space Calibration Point

Two methods were explored for employing high-altitude observations of cosmic background radiation though an approximately transparent atmosphere as a cold-space calibration point. The first method forces agreement between simulated and observed radiances at the highest altitudes from which observations were made. Model predictions at these altitudes are insensitive to small changes in modeled absorption. A 10% error in modeled attenuation through an atmosphere with mean temperature of 220 K would give rise to errors of less than 2.2 K. The second method uses scan-angle information and the fact that atmospheric opacity through a horizontal atmospheric slab is proportional to the secant of the zenith angle. Downwelling radiances at 20 km should be nearly linear in $s = \sec(\phi_{zen})$, with the extrapolated value of the cosmic background temperature at $s = 0$. These two methods typically differ by 2-3 K in the values at which they fix the highest altitude's antenna temperatures, but the resulting differences in estimated atmospheric attenuation are negligible. The sources of these discrepancies are under investigation. This second method was adopted for this analysis since it requires fewer assumptions about the atmospheric attenuation model. The method is discussed further, below.

The MPM92 model's predicted band-averaged zenith opacities from 20 km to space (modeled as 90 km) for the 118-GHz channels are less than 0.1 Np. In this transparent atmosphere limit, radiative transfer is approximately linear in opacity (τ), and it is reasonable to approximate the physical temperature of the atmosphere as a constant, T_{phys}.

$$\begin{aligned} T_B &= T_{\text{cosmic}} e^{-\tau} + T_{\text{phys}}\left(1 - e^{-\tau}\right) \\ &\cong T_{\text{cosmic}} + T_{\text{phys}}\tau \\ &\text{where} \\ \tau &\equiv \tau_{\text{zenith}} \sec\left(\phi_{\text{zenith}}\right) \end{aligned} \qquad \text{(Eqn. 6)}$$

A 10% error in modeled attenuation through an atmosphere with mean temperature of 220 K would give rise to errors of less than 2.2 K.

A second method of determining the brightness of a nearly transparent atmosphere requires no assumptions about the absorption model other than that of the transparent limit. In the transparent limit, observed brightness is an approximately linear function of τ and thus a linear function of $\sec(\phi_{zen})$. The zero intercept of this line should correspond to the intensity of the cosmic background, a 2.7 K black-body. Since 2.7 K is not small compared to $h\nu/k_B$ = 5.7 K (for ν = 118 GHz), the cosmic brightness temperature T_{cosmic}, at 118-GHz, measured in the units of high-temperature linear fit is 3.6 K. This method of using angular data to determine the cold-space calibration point has been adopted for the following analysis, and an example of how this fitting is done is shown in Figure 11. Scan data used for this fitting is limited to points with secants less than 1.4 in an attempt to minimize the effect of beam pointing uncertainty of side lobes, problems which would be expected to worsen at high angles from zenith.

The most opaque channel has enough attenuation that this linear-fit-to-secant calibration value is expected to have errors on the order of 2 K. The slopes of the fits for this channel for 20-km data are on the order of 25 K per unit secant, and in the linear-limit model, this slope is the product of τ_{zen} and $T_{phys.}$ For a nominal T_{phys} = 220 K, zenith opacity is predicted to be 0.11 Np. This is enough opacity that there are measurable departures from linearity. Inclusion of the next higher order term,

$$\left(1-e^{-\tau}\right) \cong \tau - \frac{\tau^2}{2} + \cdots$$

results in a function of brightness temperature as a function of secant of zenith angle s of the form

$$T_B(s) \cong T_{cosmic} + T_{phys}\tau_{zen}s - \frac{T_{phys}\tau_{zen}^2}{2}s^2.$$

The resulting corrections in the extrapolation to s = 0 are less than 2 K in all channels, and are included in this analysis.

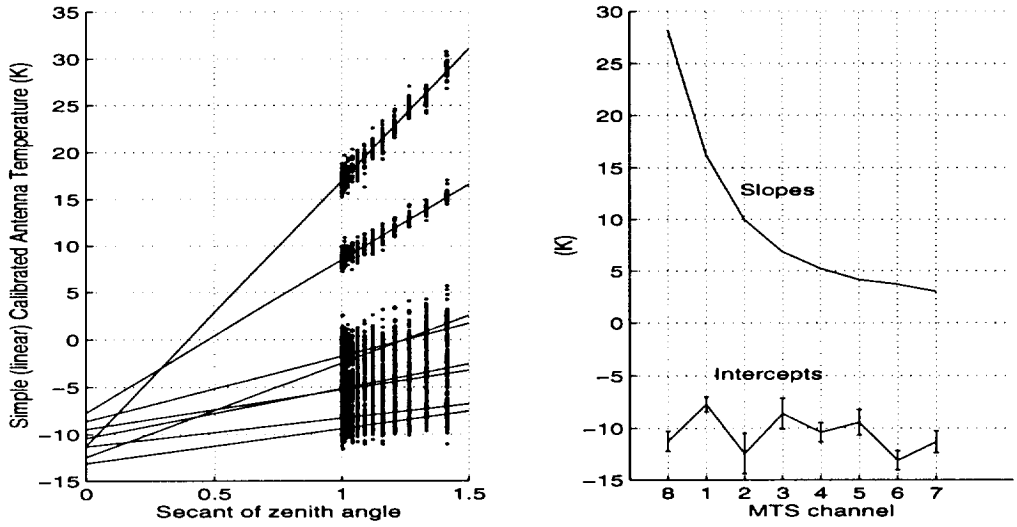

Figure 11. Data from above 19.8 km on the flight of 09-11-93. For an approximately transparent atmosphere, the zero intercepts of a linear fit of brightness to path length should be 2.7 K. This provides a model-independent calibration point

6.2.2 Application of Cold-Space Calibration to Entire Flight

The simple, two-point linear calibration based upon the MTS hot and cold loads consistently gives colder brightness temperatures for high-altitude, transparent-to-space observations than are determined using the cold-space calibration method described above. From 20 km, the simple calibration method actually results in antenna temperatures slightly below absolute zero for the most transparent channels, a clearly non-physical result. Laboratory observations of echosorb immersed in liquid nitrogen also calibrate slightly too cold by the simple method. Since the cold-space data is representative of the condition of the receiver in flight, it is preferred over laboratory measurements for use of calibration correction of flight data. A second-order calibration scheme that reasonably modifies the simple calibration scheme to reconcile discrepancies between cold-space theory and calibrated temperatures has been developed.

Two types of problems may contribute to the inadequacy of the simple, linear calibration: systematic errors in observations of the calibration loads may result in biases in the estimated linear calibration relation, and/or the instrument's response may actually be nonlinear. The gain of amplifiers tends to increase as they are cooled, and later stages may slightly saturate in flight. Since the only measurements made in flight are uncalibrated "counts" representing time-averaged differences of two output voltages of the final amplifier, the exact state of each amplifier in the ~90-dB chain is certainly not known. The memory effect discussed in Section 5.3, which results in pollution of the

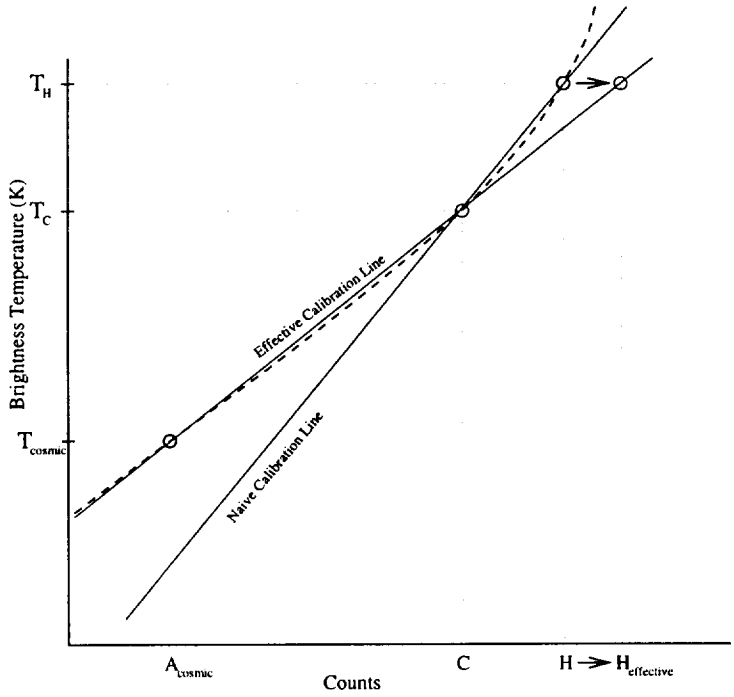

Figure 12. A fractional correction of the difference (H-C) is determined for each channel during the portions of a flight where the third, "cold space" calibration point is available. This correction is then applied to H throughout the flight.

cold-load observation with the antenna measurement to be calibrated, may be modeled with a linear and a quadratic term. A correction for estimated memory is applied to the raw data prior to calibration, but this fix is expected to be crude, and residual error may contribute to the cold-space discrepancy.

All of the proposed sources for observed large departures from simple, linear radiometer calibration of extremely cold antenna temperatures share the quality that expected errors are small near the calibration loads' temperatures and become large with extrapolation. Such errors, either due to incorrectly determined calibration slope (degrees of brightness temperature per count) or to slopes that change as brightnesses depart from the calibration load temperatures, may be corrected, to first order, by tipping the line to give reasonable calibrated radiances for the cold-space data.

The correction approach adopted is to tip the calibration line about the cold load point, modifying its slope throughout the flight by a fixed multiplicative factor selected to give agreement with the cold-space, high-altitude calibration model. The resulting modified linear calibration relation contains a first order fix both for nonlinearity and for calibration load biases. Agreement with the transparent atmosphere model is enforced for the observations which are otherwise most subject to extrapolation errors, and the corrections drop to zero as observed radiances warm to the temperature of the cold load,

where errors are expected to be small. This correction scheme treats all systematic calibration errors as errors in the hot load thermocouple measurement. The primary effect of such corrections is to tip the calibration line, and the difference between shifting the hot point or shifting the cold point to get agreement with cold space is negligible for these data sets.

The hot load is expected to be less reliable than the cold load since its large signals are more strongly affected by any amplifier nonlinearity, it is possibly subject to interference from the 53-GHz instrument (see Section 5.3), and it is farther from the antenna temperatures to be calibrated than is the cold load. If the hot calibration load is biased in such a way that it can be modeled as being some fixed fraction of the hot load temperature and the ambient temperature, then the correction adopted is precisely the correction needed. The memory effect is an example of such a case, as would be loss in the plastic covering the hot load. Nonlinearity due to amplifier saturation would be most pronounced for observations of the hot load, if counts-per-unit-intensity begins to roll off at high antenna temperatures, as in the dashed line of Figure 12.